Supplementary Information:
Size Structures Sensory Hierarchy in Ocean Life

Erik A. Martens[♯],[1,2,3] Navish Wadhwa[♯],[1,4] Nis S. Jacobsen,[1,2] Christian Lindemann,[2] Ken H. Andersen,[1,2] and André Visser[1,2]

[1]*Centre for Ocean Life*
[2]*National Institute of Aquatic Resources, Technical University of Denmark, Charlottenlund Slot, Jægersborg Alle, DK-2920 Charlottenlund, Denmark*
[3]*Department of Biomedical Sciences, Copenhagen University, Blegdamsvej 3, 2200 Copenhagen, Denmark*[*]
[4]*Department of Physics, Technical University of Denmark, DK-2800 Kgs. Lyngby, Denmark*[†]

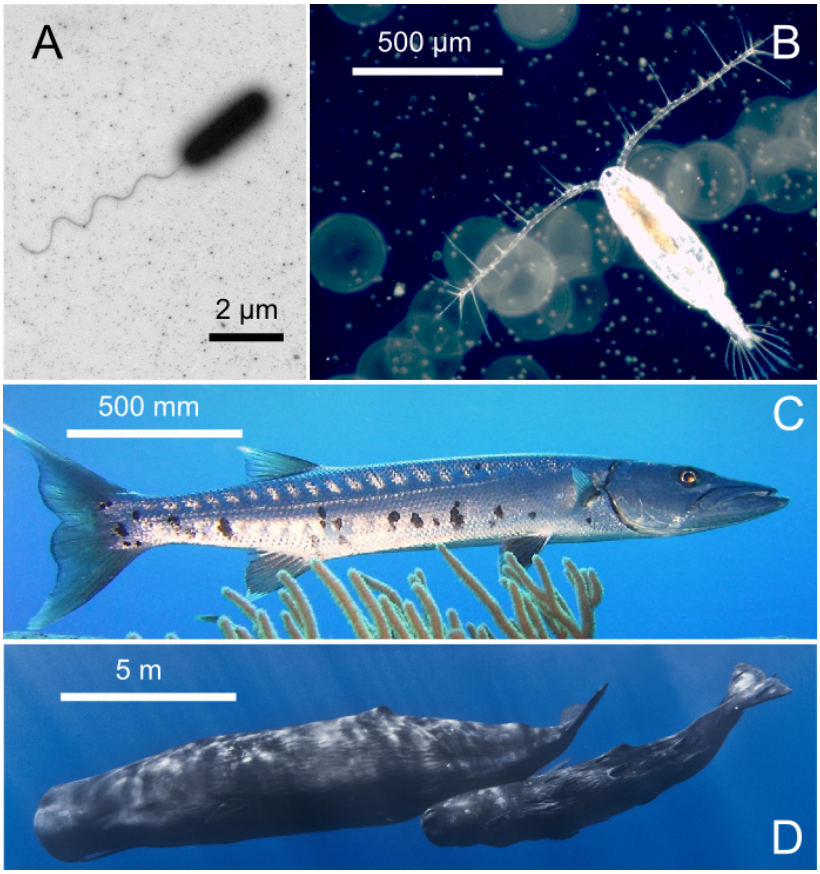

FIG. 1. Dominant sensing modes changes with increasing size of the organism: (**A**) Small organisms like bacteria (e.g., *Vibrio alginolyticus*) use chemosensing, and move up or down the gradients of chemicals (image courtesy Kwangmin Son and Roman Stocker, MIT). (**B**) Millimetre sized organisms like copepods (e.g. *Acartia tonsa*) use hydromechanical signals to detect predators and prey in the vicinity (image courtesy of Thomas Kiørboe, DTU). (**C**) Larger organisms like fish (e.g. great barracuda *Sphyraena barracuda*) are often visual predators. (**D**) Toothed whales (e.g. *Physeter macrocephalus*) use echolocation. Images in panels C,D are in public domain.

I. CHEMOSENSING

A. A note on chemical contrast

An absolute upper limit on sensing range is dictated by the requirement of sufficient chemical contrast. Chemosensing requires spatial variations in signal strength that can be detected and gradients therein tracked. However, chemical gradients

[*] Equal contribution.; erik.martens@sund.ku.dk
[†] Equal contribution.; nawa@fysik.dtu.dk

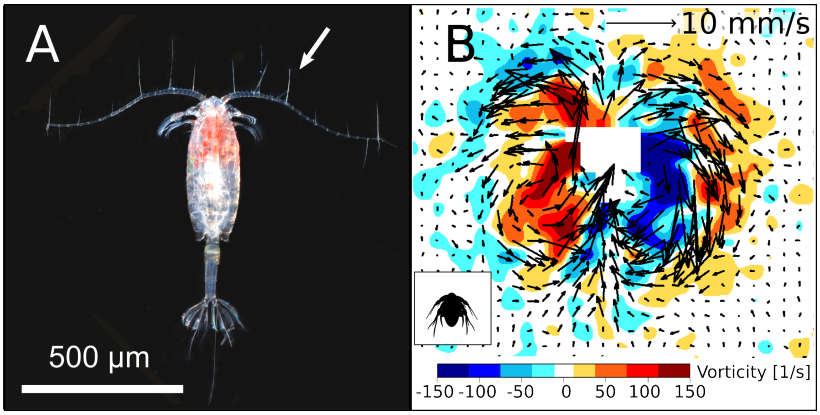

FIG. 2. **Mechanosensing. A:** Dorsal view of an adult *Acartia tonsa*, showing the antennules covered with mechanosensory setae, one of which is marked with an arrow (image courtesy of Erik Selander). **B:** Flow disturbance created by a swimming *Acartia tonsa* nauplius, visualized in the form of velocity vectors and vorticity contours.

tend to become eroded with time to background level. The upper limit chemosensing range is not only related to the size and sensory ability of the organism, but also to the nature of the chemical substrate and its degradation in the environment due to microbial action or chemical reactions. Thus, while it is clear that an upper limit to chemosensing range exists, it is not possible to quantify it.

II. VISION

A. Size limit for compound eyes

The compound eye is hemi-spherical in shape and subdivided into light-detecting units called *ommatidia*. Ommatidia are conical in shape and cover the surface with an opening of width δ. Given that the eye has a radius r, the visual acuity of an ommatidium is given by

$$\Delta\phi = \delta/r. \tag{1}$$

The number of ommatidia covering the hemispherical eye surface may be estimated as the ratio of the eye surface, around $2\pi r^2$, and the surface element covered by an ommatidium, around $r^2\Delta\phi^2$,

$$N = \frac{2\pi r}{\Delta\phi^2}. \tag{2}$$

Increasing the number of ommatidia, N, enlarges the image-resolution of the eye; however, as δ is decreases, diffraction effects becomes increasingly important. Thus, minimization of ommatidia in compound eyes is limited due to diffraction limits, see [1, 2]. Considering this trade-off, the optimal width of the ommatidia can be estimated [1], yielding

$$\delta = \sqrt{\lambda r}, \tag{3}$$

where $\lambda = 400$nm is the wave length of blue light.

Substituting Eqs. (1) and (3) into Eq. (2), we obtain the resolution of an eye with optimal ommatidia, we have

$$N = \frac{2\pi r}{\lambda}. \tag{4}$$

The size of an optimal compound eye is then

$$L_{\text{eye}} = 2r = \frac{\lambda N}{\pi}. \tag{5}$$

The size of the optimal compound eye with a reasonably useful resolution of $N = 100^2$ pixels should be $L_{\text{eye}} = 1.2$ mm, corresponding to roughly $L \sim 1$ to 3 cm (depending on the size ratio of eye to body). By comparison, some of the smallest organisms carrying compound eyes are *Daphnia*, with adults ranging from 1 to 5 mm [3]. Optimality of the eye, Eq. (5), then implies a resolution of $N \sim 10^2$ pixels – however, this is a resolution which barely produces a usable image.

B. Sensing range

The sensing range condition in the main text is given by

$$C_0 e^{-\alpha R} \geq C_{\rm th,min} + K R^2 L^{-4}. \tag{6}$$

Rescaling the sensing range, $\tilde{R} = \alpha R$ and the size, $\tilde{L} = (C_0 \alpha^2 / K)^{1/4}$ where $C := C_{\rm th,min}/C_0$, this becomes

$$e^{-\tilde{R}} \geq C + \tilde{R}^2 \tilde{L}^{-4}. \tag{7}$$

The clear-water limit corresponds to small $\tilde{R} \ll 1$, yielding

$$\tilde{R} \sim \tilde{L}^2 (1-C)^{1/2}, \tag{8}$$

and the turbid-water corresponds to large $\tilde{L}$, yielding

$$\tilde{R} \sim -\ln(C)/\alpha. \tag{9}$$

These expressions match the ones presented in the main text.

Letting the two expressions for the rescaled sensing ranges (8) and (9) be similar, we arrive at the condition for the cross-over between the two regimes:

$$\tilde{L}_x^2 \sim -\ln(C)/(1-C)^{1/2}, \tag{10}$$

which in the original unscaled variables becomes $L_{\rm x}^2 \sim \alpha^{-1} K^{\frac{1}{2}} (C_0 - C_{\rm th,min})^{-\frac{1}{2}} \ln(C_0/C_{\rm th,min})$ or, to leading order,

$$L_{\rm x}^2 \sim \alpha^{-1} K^{\frac{1}{2}} (C_0 - C_{\rm th,min})^{-\frac{1}{2}}. \tag{11}$$

The clear-water limit occurs for $L \ll L_x$ and the turbid water limit for $L \gg L_x$. Thus, the turbid limit is reached in the limit of large α, large $(C_0 - C_{\rm th,min})$, or small sensitivity K, respectively.

Another (rough) estimate of the minimal body size, for which vision is still marginally meaningful, might be feasible from the condition that $L \sim R$. This condition has at most two solutions, whereas the minimal solution is $L \approx [K/(C_0 - C_{\rm th,min})]^{1/2}$. A precise determination of this estimate of the smallest animal carrying an eye is, however, difficult due to the unknown scaling coefficient in this estimate and uncertainties concerning parameter values.

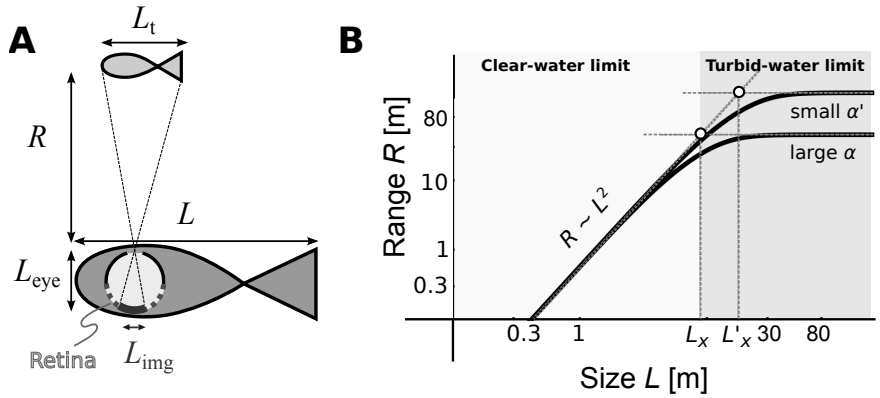

FIG. 3. **Vision.** **A**: An organism of body size L, with an eye of size $L_{\rm eye}$, detects a target of size L_t at a distance R if the apparent contrast of the target is equal or larger than the threshold contrast of the organism's eye. **B**: Maximal visual sensing range scales with body size L: like $R \sim L^2$ in the clear-water limit ($L \ll L_x$) and like $R \sim$ constant in the turbid-water limit ($L \gg L_x$). Parameters are $K = 0.025, C_0 = 0.3, C_{\rm th,min} = 0.05$ (adopted from [4]), $\alpha = 0.04$ m^{-1} [5] (α' = 0.01 m^{-1} for comparison) and $a = 1:30$.

III. ECHOLOCATION

A. Scaling argument for sensing range

We estimate how the range of echolocation scales with body size L based on three assumptions: i) the threshold sensitivity of the ear I_0 is independent of organism size L [6], ii) the emitted sound intensity I_e scales with size: $I_e \propto L^{3\phi}$ where $3/4 < \phi < 1$, and iii) the carrier frequency of the signal depends on L (see [7]).

The generated acoustic signal first travels through water, is then partially reflected by the target, and the remainder of the signal travels back to the organism. I_e, is thus reduced by two processes:

i) ***Reflection.*** The signal is reduced upon reflection from the target and the reflected intensity is proportional to the target area which scales as L_t^2.

ii) ***Attenuation.*** Sound intensity decreases with distance as r^{-2} due to geometric divergence. It is further attenuated exponentially due to absorption in the seawater.

Together, the signal intensity attenuates as $(2r)^{-2}e^{-2\mu r}$, where the factor 2 is due to the doubled travel distance. Geometric attenuation strongly dominates over the absorption processes, thus, $I_r \sim I_e L_t^2 r^{-2} \sim L^{3\phi} L_t^2 r^{-2}$. The strength of the returned signal must exceed the threshold intensity for detection in the ear, $I_r = I_0$, yielding a sensing range $R \sim I_0^{-1/2} L^{3\phi/2} L_\mathrm{t}$. Introducing the size ratio $p = L_\mathrm{t}/L$, we arrive at

$$R \sim p I_0^{-1/2} L^\gamma, \tag{12}$$

where the exponent $\gamma = 1 + 3\phi/2$ lies between 2.125 to 2.5. The scaling factor depends on unknown parameters, but can be estimated from data describing the echolocation range of small marine mammals. The resulting scaling coefficient (including p/I_0) is 6.47 $\mathrm{m}^{-1.5}$ for $\gamma = 2.5$, and 9.79 $\mathrm{m}^{-1.125}$ for $\gamma = 2.125$.

Figure 5 compares the scaling for Eq. 12 with data available for dolphins [8–12]. There is considerable scatter in the data, yet we recognize that the prediction compares with the data reasonably well.

1. Signal attenuation

We detail our estimates for the effects of attenuation due to geometric divergence and absorption processes in sea water. First, we discuss the effect of absorption processes on the transmission of pulses. To begin, we note that the absorption coefficient μ is frequency dependent. Each pulse is transmitted and characterized by its center (or carrier) frequency f_c, which is also the dominant frequency of the pulse spectrum. We may disregard all other frequencies and thus the dispersion of the transmitted pulse, leaving us with the task to find the absorption coefficient for f_c. The attenuation of sound in seawater is a complex molecular process which occurs both due to viscous absorption generated by particle motion, but also due to molecular relaxation processes by Boric acid and Magnesium sulphate. A formula for the frequency dependent absorption has been devised [13]. However, this relation is too complicated for our purposes as we desire to establish a simple asymptotic scaling relation between f_c and μ; indeed, the data is well *parameterized* by $\mu \sim f_c^{4/3}$ (see Section 3 below and Figure 5). Further, it is known that f_c depends on body size; experimental data [7] for dolphins (excluding river dolphins), allows us to heuristically deduce a scaling dependence for the absorption, $f_c \approx 370\ \mathrm{m}^{3/4}\ \mathrm{s}^{-1} \times L^{-3/4}$ (see Section 2 below). Combining these two scalings, we obtain for the absorption coefficient (decibel / meter) $\mu \approx 10^{-2} L^{-1}$. Finally, since the fitted data is measured in the logarithmic decibel scale, the attenuation factor due to absorption converts to $10^{-0.1\mu(L)\times 2R}$. Summed up, the intensity is reduced by a factor $I_r/I_e \sim R^{-2} 10^{-0.001\times 2R/L}$. However, further analysis shows that the effect of damping is negligible when compared to the geometric divergence. Thus, the reflected sound intensity simplifies to $I_r \sim L^{3\phi} L_o^2 R^{-2}$.

2. Center frequency

Center frequencies of echolocation signals have been measured for dolphins [7], shown in Figure 4A. The two river dolphins discussed in [7] are excluded from our analysis, since dolphins in such environments operate at different frequencies to adapt for sound transmission in non-free environments. We fitted the relation between the body mass w and the center frequency by $f_c \approx (368.7\ \mathrm{m}^{0.26}\ \mathrm{s}^{-1}) \times m^{-0.26}$. Since the mass scales as $w \sim L^3$, we obtain $f_c \sim L^{-3/4}$.

For comparison, note that the frequency with maximal intensity produced in the nasal sac is approximated by the Helmholtz frequency [14]:

$$f_p = \frac{c}{2\pi} \left(\frac{A}{V\ L_\mathrm{t}} \right)^{1/2} \propto L^{-1}. \tag{13}$$

where A, V, L_t are the area, volume and length of the nasal sac. Given that m is proportional to L^3, the scaling observed in Fig. 4 appears to deviate somewhat from this theoretical estimate. The deviation may be explained by shortcomings of the simple Helmholtz oscillator model.

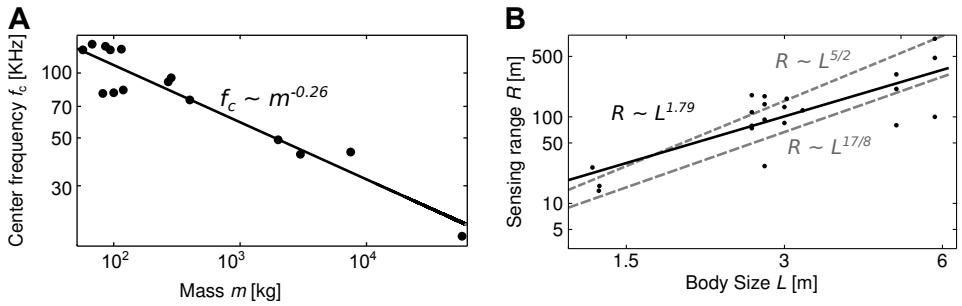

FIG. 4. **Echolocation.** **A:** Power law fit for echolocation center frequencies of dolphins. Data from [7]: f_c = (17.5, 42, 43, 75, 49, 95, 83.4, 80.4, 91, 81, 128, 136, 129, 133, 128) kHz; m = (57000, 3000, 7500, 400, 2000, 285, 119, 82, 270, 100, 94, 67.5, 115, 86, 57) kg. **B:** Comparison of the predicted echolocation sensing range (dashed grey) with data (black dots), which scales like $R \approx 14.2\ \mathrm{m}^{-0.79} \cdot L^{1.79}$ (black line, least squares fit).

3. *Sound absorption in marine environments*

The authors in [13] derive a simplified equation of the form

$$\mu = A_1 P_1 f_1 f_c^2/(f_1^2 + f_c^2) + A_2 P_2 f_2 f_c^2/(f_2^2 + f_c^2) + A_3 P_3 f_c^2 \tag{14}$$

where the center frequency f_c is measured in Hz at the depth z in km. Further, they determine the following coefficients characteristic to the properties of seawater for boron and for magnesium,

$$\begin{aligned} f_1 &= 0.78 * (S/35)^{1/2} e^{T/26} \\ f_2 &= 42 e^{T/17} \\ A_1 &= 0.106 \\ A_2 &= 0.52 * (1 + T/43)(S/35) \\ A_3 &= 0.00049 \\ P_1 &= e^{(pH-8)/0.56} \\ P_2 &= e^{-z/6} \\ P_3 &= e^{-(T/27+z/17)}. \end{aligned}$$

Location	pH	S [ppt]	T [C]	z [km]
Pacific	7.7	34	4	1
Red Sea	8.2	40	22	0.2
Arctic Ocean	8.2	30	-1.5	0
Baltic Sea	7.9	8	4	0

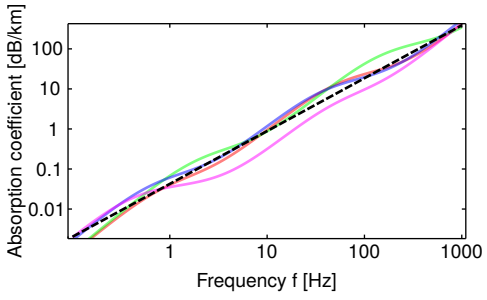

FIG. 5. Power law fit for relation between frequency and sound absorption coefficient in the ocean. **Top:** Parameter values for pH, S, T, z for Eq. 14 valid for different ocean regions. **Bottom:** Absorption rates resulting from parameters for the various regions listed in the top table. Fitting the logarithmic data linearly (dashed line) over the frequency range of interest results in the asymptotic scaling relation μ [db/km] $\approx 0.0434\ \mathrm{s}^{-4/3}\mathrm{km}^{-1} \times f^{4/3}[\mathrm{s}^{-1}]$.

The scaling for the absorption coefficient μ is thus (decibel per meter)

$$\mu \approx 4.2 \times 10^{-5} \mathrm{s}^{4/3} \mathrm{m}^{-1} \times f_c^{4/3}. \tag{15}$$

where the center frequency (s^{-1}) is

$$f_c \approx 65.8\, \mathrm{s}^{-1} \mathrm{m}^{3/4} \times L^{-3/4} \tag{16}$$

where we have used the relation mass w = ρL^3 with $\rho = 10^3$ kg m^{-3}. Thus, we obtain (decibel per meter)

$$\mu \approx 10^{-2} \times L^{-1}. \tag{17}$$

B. Assumptions underlying the scaling argument

The scaling argument for the range rests on assumptions supported by data only in part, which we review here for clarity:

(A1) the threshold sensitivity of the ear I_0 is independent of target size L. This approximation is supported by audiograms (behavioral and auditory brain stem responses) of odontocetes [12, 15–18],

(A2) the emitted sound intensity that an animal produces scales with size: $I_e \propto L^{3\phi}$ where $3/4 < \phi < 1$,

(A3) the carrier frequency of the sonar signal depends on size L.

Assumption (A3) seems fairly well corroborated, as already discussed in section A and B. Assumption (A2) states that the scaling exponent ϕ is allowed to vary in a small range corresponding to a sublinear volume dependence of the generating organ size which is a fairly reasonable assumption. Taking into account the considerable scatter of the data, we recognize that the prediction compares with the data reasonably well, as is evidenced in Figure 7 in the main text. However, better data is required to further underpin assumption (A1). Indeed, within the group of whales and dolphins we find no clear *size*-dependence for the sensitivity threshold I_0 [18]; but it would be desirable to obtain more data to solidify this assumption, as well as to identify a satisfactory physical or biological explanation for why the sensitivity is independent of body size, in contrast to other mammal groups [15–19].

[1] Feynman, R. P., 2013 Color vision. In *The Feynman Lectures on Physics* (eds. M. A. C. Gottlieb & R. C. Pfeiffer), chapter 36.4. California Institute of Technology.

[2] Land, M., 1997 Visual acuity in insects. *Annual Review of Entomology* **42**, 147–177. ISSN 0066-4170. (doi: 10.1146/annurev.ento.42.1.147).

[3] Ebert, D., 2005 *Ecology, Epidemiology, and Evolution of Parasitism in Daphnia*. Bethesda (MD): National Center for Biotechnology Information (US).

[4] Dunbrack, R. & Ware, D., 1987 Energy constraints and reproductive trade-offs determining body size in fishes. In *Evolutionary Physiological Ecology* (ed. P. Calow), pp. 191–218. Cambridge University Press.

[5] Beckmann, A. & Hense, I., 2007 Beneath the surface: Characteristics of oceanic ecosystems under weak mixing conditions – a theoretical investigation. *Progress in Oceanography* **75**, 771–796. ISSN 00796611. (doi:10.1016/j.pocean.2007.09.002).

[6] Ketten, D. R., 2004 Marine mammal auditory systems: A summary of audiometric and anatomical data and implications for underwater acoustic impacts. *Polarforschung* **72**, 79–92.

[7] Jensen, F. H., Rocco, A., Mansur, R. M., Smith, B. D., Janik, V. M. & Madsen, P. T., 2013 Clicking in shallow rivers: Short-range echolocation of irrawaddy and ganges river dolphins in a shallow, acoustically complex habitat. *PloS one* **8**, e59284. ISSN 1932-6203. (doi:10.1371/journal.pone.0059284).

[8] Au, W. & Snyder, K., 1980 Long-range target detection in open waters by an echolocating atlantic bottlenose dolphin (tursiopstruncatus). *The Journal of the Acoustical Society of* ... pp. 1077–1084.

[9] Barrett-Lennard, L. G., Ford, J. K. & Heise, K. A., 1996 The mixed blessing of echolocation: Differences in sonar use by fish-eating and mammal-eating killer whales. *Animal Behaviour* **51**, 553–565. ISSN 00033472. (doi:10.1006/anbe.1996.0059).

[10] Kastelein, R. A., Au, W. W., Rippe, H. T. & Schooneman, N. M., 1999 Target detection by an echolocating harbor porpoise (phocoena phocoena). *The Journal of the Acoustical Society of America* **105**, 2493–2498. ISSN 0001-4966.

[11] Murchison, A. E., 1980 *Animal Sonar Systems*. Boston, MA: Springer US.

[12] Teilmann, J., Miller, L. A., Kirketerp, T., Kastelein, R. A., Madsen, P. T., Nielsen, B. K. & Au, W. L., 2002 Characteristics of echolocation signals used by a harbour porpoise (*Phocoena phocoena*) in a target detection experiment. *Aquatic Mammals* **28**, 275–284. ISSN 01675427.

[13] Ainslie, M. & McColm, J., 1998 A simplified formula for viscous and chemical absorption in sea water. *The Journal of the Acoustical Society of America* **103**, 1997–1998.

[14] Aroyan, J., McDonald, M., Webb, S., Hildebrand, J., Clark, D., Laitman, J. & Reidenberg, J., 2000 Acoustic models of sound production and propagation. In *Hearing by Whales and Dolphins*, 2000.

[15] Nachtigall, P. E., Mooney, T. A., Taylor, K. a. & Yuen, M. M. L., 2007 Hearing and auditory evoked potential methods applied to odontocete cetaceans. *Aquatic Mammals* **33**, 6–13. ISSN 01675427. (doi:10.1578/AM.33.1.2007.6).

[16] Pacini, A. F., Nachtigall, P. E., Kloepper, L. N., Linnenschmidt, M., Sogorb, A. & Matias, S., 2010 Audiogram of a formerly stranded long-finned pilot whale (globicephala melas) measured using auditory evoked potentials. *The Journal of Experimental Biology* **213**, 3138–3143. ISSN 0022-0949. (doi:10.1242/jeb.044636).

[17] Pacini, A. F., Nachtigall, P. E., Quintos, C. T., Schofield, T. D., Look, D. a., Levine, G. a. & Turner, J. P., 2011 Audiogram of a stranded blainville's beaked whale (mesoplodon densirostris) measured using auditory evoked potentials. *The Journal of Experimental Biology* **214**, 2409–15. ISSN 1477-9145. (doi:10.1242/jeb.054338).

[18] DOSITS.org, 2014 What sounds can animals hear? *Discovery of Sound in the Sea (dosits.org)* .

[19] Kastelein, R. A., Bunskoek, P., Hagedoorn, M., Au, W. L. & de Haan, D., 2002 Audiogram of a harbor porpoise (phocoena phocoena) measured with narrow-band frequency-modulated signals. *The Journal of the Acoustical Society of America* **112**, 334. ISSN 00014966. (doi:10.1121/1.1480835).